Title

Estimation of Line Cross Sections Using Critical-Dimension Grazing-Incidence Small-Angle X-Ray Scattering

Journal

Physical Review Applied, 12(4)

ISSN

2331-7043

Authors

Freychet, Guillaume
Kumar, Dinesh
Pandolfi, Ron J
et al.

Publication Date

2019-10-01

DOI

10.1103/physrevapplied.12.044026

Peer reviewed

Estimation of line cross-sections using critical dimension grazing incidence small angle X-ray scattering

Guillaume Freychet,[1] Dinesh Kumar,[2,*] Ron J. Pandolfi,[3] Patrick Naulleau,[4] Isvar Cordova,[5,†] Peter Ercius,[6] Chengyu Song,[6] Joseph Strzalka,[7] and Alexander Hexemer[5,‡]

[1] *NSLS-II, Brookhaven National Laboratory*

[2] *Center for Advanced Mathematics for Energy Research Applications, Lawrence Berkeley National Laboratory*

[3] *Center for Advanced Mathematics for Energy Research Applications, Lawrence Berkeley National Laboratory*

[4] *Center for X-ray Optics, Lawrence Berkeley National Laboratory*

[5] *Advanced Light Source, Lawrence Berkeley National Laboratory*

[6] *Molecular Foundary, Lawrence Berkeley National Laboratory*

[7] *X-ray Science Division, Advanced Photon Source Argonne National Laboratory*

Abstract

The semiconductor industry is continuously pushing the limits of photolithography, with feature sizes now under 10 nm. In order to ensure quality, it has become necessary to look beyond the conventional metrological techniques. X-ray scattering has emerged as a possible contender to determine the average shape of a line grating with a sub-nanometer precision. However, to fulfill its promise, faster algorithms must also be developed to interpret and extract metrics from reciprocal space scattering data. In this paper, we are presenting a novel, fast, and accurate X-ray technique and analysis algorithm: critical dimension grazing incidence X-ray scattering, *CD-GISAXS*. The CD-GISAXS technique operates in grazing incidence configuration with a continuous azimuthal rotation of the sample, thus does not require high-energy X-rays to penetrate the wafer and greatly reduces the data acquisition times, permitting analysis within the framework of the Distorted-Wave Born Approximation (DWBA).

I. INTRODUCTION

Lithographically manufactured nanostructures continue to shrink in size in a struggle to keep pace with Moore's Law. The semiconductor industry is exploring new metrology techniques capable of meeting the future requirement to characterize three-dimensional structure with sub-10 nm critical dimensions. Direct imaging techniques such as Scanning Electron Microscopy (SEM) and Scanning Force Microscopy (SFM), and indirect imaging techniques such as X-ray Optical Critical Dimension (OCD) scatterometry have been the state of the art when it comes to characterization of these structures [1–4]. All these approaches propose a way to probe nano-objects in depth, but are either approaching their resolution limits or are too slow for in-line measurements.

Therefore, the semiconductor industry is looking to supplement the metrology techniques. Several promising alternatives were listed in the International Technology Roadmap for Semiconductors (ITRS) [5]. One of them is the X-ray scattering technique. Combined with the advent of high brightness sources, faster detectors, and advances in mathematical treatment of scattering data, there is a real possibility for combining fast X-ray acquisition

* dkumar@lbl.gov

† Center for X-ray Optics, Lawrence Berkeley National Laboratory

‡ ahexemer@lbl.gov

with high-speed data treatment in order to reach the timescales required for an effective in-line characterization method. One of the pioneering techniques, called Critical-Dimension Small Angle X-ray Scattering (CD-SAXS), has been developed at the National Institute of Standards and Technology (NIST) over the last few years and has demonstrated the ability of X-ray scattering to reconstruct line profiles with sub-nanometer resolution [6, 7]. CD-SAXS is a variable-angle transmission scattering measurement where the sample is rotated to probe the vertical profile. The recent success of the use of iterative algorithms on CD-SAXS data, more precisely a genetic algorithm coupled with a Monte-Carlo Markov-Chain (MCMC) approach, have led to a precise reconstruction of the line profile's depth from a stack of trapezoids [8, 9]. The approach has been extended to the study of polymer gratings and line edge roughness [10–12].

Conducting such measurements in a transmission configuration imposes stringent requirements of high-energy and high-flux in order for the X-rays to penetrate through silicon wafers, presenting a limitation of CD-SAXS. It is a tough condition to meet, sometimes even for the modern state-of-the-art in-line sources. The attenuation through silicon substrates can force the need for longer exposure times. However, applying this technique in combination with the use of reflection or "Grazing Incidence" geometry can overcome this limitation of traditional CD-SAXS; we will present such a combined approach here.

Grazing Incidence Small Angle X-ray Scattering (GISAXS) is mostly used for the characterization of thin film morphologies, but has been recently used to approximate the profile of polymer line gratings [13]. A precise alignment of the lines in the direction of the incoming beam is required to record a semicircle of spots, which are laid out as the intersection of the Ewald sphere with the Bragg rods from the gratings [14, 15]. This allows the pitch of the gratings to be extracted from the position of the Bragg spots on the semicircle. In order to reconstruct the whole line profile, several approaches were developed. The first axis of development was the experimental one, aiming to collect more information from the line profile. To do so, Hoffman *et al.* proposed to rotate the gratings along the normal of the substrate to record the full Bragg rods [16]. Later on, Suh *et al.* proposed to record GISAXS images at several incident angles to probe the form factor of the line profile across different regions of reciprocal space [13]. In parallel, development improving data analysis progressed. Transmission scattering in grazing-incidence geometry, called GT-SAXS, were studied to get rid of the complexity of the distorted-wave Born approximation (DWBA) formalism [17]. A

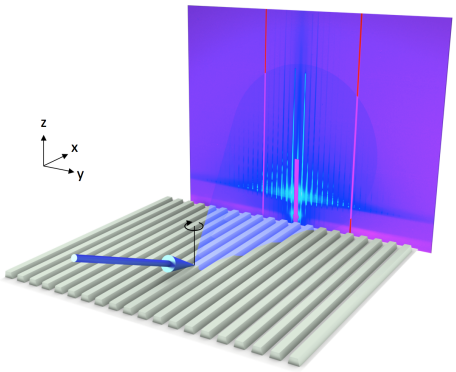

FIG. 1: Grazing-incidence small angle X-ray scattering with the beam along x-axis and the sample rotation along z-axis.

3D reconstruction of the line profile in the frame of DWBA was proposed by Soltwisch et al. [18] by solving the Maxwell equations using finite elements. Most recently, Suh *et al.* proposed a model to extract the roughness of line gratings with a combination of AFM and GISAXS [13].

Here, we extend the GISAXS approach[16] proposed by Hoffman *et al.*, with a continuous rotation of the sample stage, to fit for the first time the form factor along several full Bragg rods — a novel and more holistic approach. The robustness of the fit was thus improved by increasing the number of experimental data points. The development of a genetic algorithm led to the reconstruction of the line profile as a stack of trapezoids with sub-nanometer resolution [19, 20]. The extracted line profile is then compared with cross-section TEM results.

II. CD-GISAXS MEASUREMENTS

A. Sample preparation

CD-GISAXS measurements were done on a 300-mm wafer samples, provided by a leading semiconductor manufacturer and exposed on an ASML 193 immersion tool. The lines are made of resist with a nominal pitch of 87.6 nm. The patterned area is 10×20 mm^2.

B. Cross-section TEM

The focused ion beam (FIB) *ex situ* liftout procedure [21] was used to extract cross-sectional specimens of the line patterns for characterization via scanning transmission electron microscopy (STEM). We used a Thermo Fischer Helios G4 operated by the National Center for Electron Microscopy (NCEM) facility of the Molecular Foundry. First, a layer of Pt was deposited with the electron beam onto the resist gratings in order to protect the exposed resist from the Ga^+ ion beam. Then, a second thicker layer of Pt was deposited using the ion beam. The resulting sample lamella was attached to a Cu grid for further thinning to electron transparency using a 1 kV Ga^+ beam to remove FIB damage. More images of the sample and liftout procedure are available in the Supplementary material. High resolution images of the cross-sectioned sample were then acquired using NCEM's Thermo Fischer Themis 60-300 operated in STEM mode. The images were acquired using a high-angle annular dark field detector, 300 kV accelerating voltage, 10 mrad convergence angle and 15 pA of beam current.

C. CD-GISAXS

CD-GISAXS experiments were performed at beamline 8-ID-E of the Advanced Photon Source. A Pilatus 1M was positioned at 2.19 m of the sample and the beamline energy was set at 10.915 keV. The incident angle was set at 0.16 deg, between critical angles of the silicon (0.165 degree) and the resist (0.12 degree). The 10×5 mm^2 etched pattern is mounted on the center of rotation of the beamline spin-coater [22], such that the incoming beam is incident on the plane of the etched lines at 0.16°. Samples were rotated about the axis normal to the substrate as illustrated on figure 1. The footprint of the beam is several centimeters, thus the whole etched area will illuminated during the measurement. The wobbling effect introduced by the rotation of the spin-coater was quantified on the beamline by comparing results between two x-ray reflectivity measurements of a polymer thin film sample performed under static and rotation configurations. The results showed a slight broadening of the Kiessig fringes, but the broadening effect on the FWHM was contained to below 5%.

The Fourier rods coming from the gratings, also known as Bragg rods, intersect with the

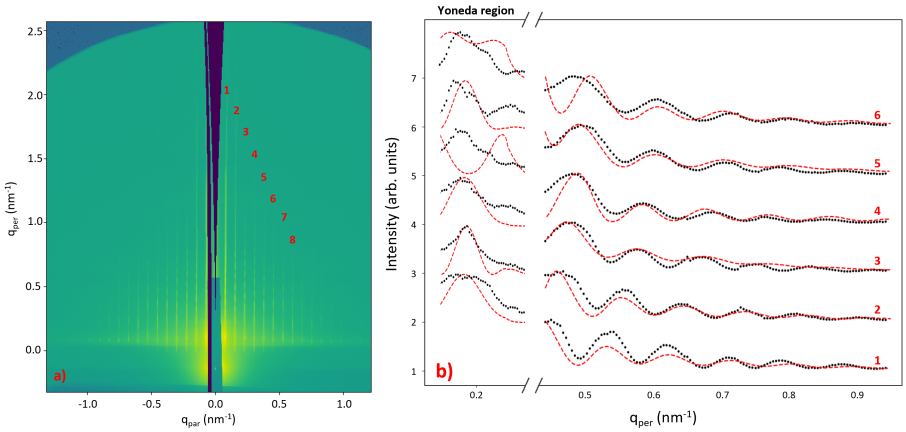

(a) (b)

FIG. 2: a) CD-GISAXS images recorded with a rotation of the gratings under the beam and b) the corresponding $q_\perp$ profiles obtained from 1D cuts along the Bragg rods.

momentum transfer vector of the elastic X-ray scattering at a single point above the horizon. The Bragg rods can be scanned by rotating the momentum transfer vector, and therefore the sample. The GISAXS image, shown in figure 2, was recorded with a 100 s acquisition time with the sample rotating at 500 rpm during the acquisition. The experimental data was remeshed into the reciprocal space, explaining the absence of data at $q_\parallel = 0$ nm^{-1}. The intensity of the recorded Bragg rods is modulated by the Fourier transform of the shape, i.e. the form factor of the individual grating lines are visible with line-cuts along the Bragg rods. Each profile is indexed and shown in figure 2b. Therefore, as for di-block co-polymers, these modulations are providing in-depth information, and are more precisely coming from the in-depth profile of the line [23]. Moreover, the full rotation of the sample, 360 degrees, overcoming the need for precise alignment of the line with regards to the beam. In absence of the aforementioned setup, a sub-degree alignment is needed for GISAXS measurements.

III. THEORY

In this section we will discuss the theoretical model used in simulation of the form-factor and subsequent reconstruction of the line shapes. The Distorted Wave Born Approximation (DWBA) is commonly used when it comes to modeling grazing incidence scattering events. The sample is approximated as a ridge repeated at regular intervals in a 1-D lattice, so

scattering gets you the form-factor of the ridge sampled by the structure factor from the lattice, and we observe the intersection of this with the idealized Ewald sphere projected onto the plane of the detector, resulting in small spots arranged in a semicircle when the ridges are parallel to the beam [13]. When the sample is rotated *in-plane* during the GISAXS measurement these spots move along the *z-axis*, while staying stationary in the *y-axis*, in reciprocal space. The final scattering image contains high intensity continuous vertical lines. These lines are modulated by the form-factor. Assuming that line shape does not vary significantly, we can simulate these vertical lines using DWBA. A similar pattern can be achieved by continuously changing the angle of the incident beam, but this increases the complexity of the algorithm, because the coordinate values are changing for every change in the incident angle (1). The simulations for all the incident angles in the range need to be in the detector coordinate system before they can be added and compared to the scattering data.

$$\begin{Bmatrix} q_x \\ q_y \\ q_z \end{Bmatrix} = \frac{2\pi}{\lambda} \begin{pmatrix} \cos\alpha\cos\theta - \cos\alpha_i \\ \cos\alpha\sin\theta \\ \sin\alpha + \sin\alpha_i \end{pmatrix} \tag{1}$$

A. DWBA

DWBA extends the Born approximation to include both reflective and refractive events to compute the scattering. Under the assumptions of stratified media, Maxwell's electromagnetic equations can be reduced to Helmholtz's equations. The resulting homogeneous equations can be solved exactly using the Green's function. Instead of deriving the DWBA, we will refer the reader to these publications [24, 25] for a detailed discussion on the topic. Similar to the Born approximation, where detector intensity is proportional to the absolute squared value of the Fourier transform of the electron density of the scatterer, DWBA stipulates that intensity is proportional to the absolute squared value of the summation of four scattering events, see figure 3 and equation (2). There are software tools, such as HipGISAXS, BornAgain, and IsGISAXS, etc, available to calculate GISAXS patterns [26, 27].

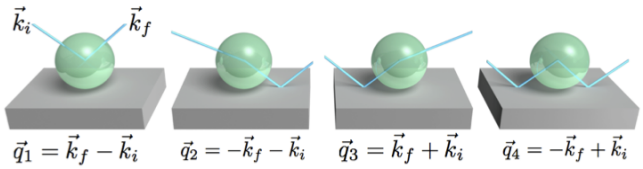

FIG. 3: Four terms involved in the scattering in the frame of the DWBA. The first term corresponds to the simple Born approximation. The higher order terms are reflecting the impact events at the silicon substrate interface.

$$I(q_\parallel, q_\perp) \propto \left|\mathcal{F}(q_\parallel, q_\perp)\right|^2, \tag{2}$$

$$\mathcal{F}_i(q_\parallel, q_\perp) = \sum_{j=1}^{4} C_i\left(\alpha^f, \alpha^i; \eta, t\right) F_i\left(q_x, q_y, \pm k_z^f \mp k_z^i; \ell\right) \tag{3}$$

where, C_i is the Fresnel coefficient for a given medium with a complex refractive index η and thickness t. F_i is the Fourier transforms of a shape with dimensions ℓ. $q_\parallel$ and $q_\perp$ have their usual meaning. If the medium is air (or vacuum), i.e. $\eta = 0$, the calculation Fresnel coefficients is simplified to:

$$\begin{aligned} C &= [1, r(\alpha^i), r(\alpha^f), r(\alpha^i) r(\alpha^f)]^T, \\ r &= \frac{k_z - \tilde{k}_z}{k_z + \tilde{k}_z}, \\ \tilde{k}_z &= -\sqrt{\eta_s^2 k_0^2 - |k_\parallel|^2} \end{aligned}$$

where η_s is complex refractive index of the substrate.

B. Simulation of the form-factor

If we assume that the etched line gratings are infinitely long, the mathematical problem of resolving the shape of the gratings is reduced to a 2-D cross-section. The cross-section of line gratings can be approximated by stacking multiple trapezoids. In order to simplify the description of the line profile, the trapezoids' heights, h, are kept identical for each trapezoid. Moreover, each trapezoid is symmetric, with both of it side-wall angles equal. Each trapezoid is therefore describe by a sidewall angle β, a height h and a bottom width L as illustrated in figure 4. The Fourier transform of each trapezoid can be expressed as:

$$F(q_y, q_z) = \frac{1}{q_y}\left[-me^{jh\frac{q_y L}{2}}\left(1 - e^{-jh\frac{q_y + m\,q_z}{m}}\right) + me^{-jh\frac{q_y L}{2}}\left(1 - e^{-jh\frac{q_y + m\,q_z}{m}}\right)\right]$$

where m is the tangent of the sidewall angle. The Fourier transform of the tessellation is given as:

$$\mathcal{F} = \sum_{n=0}^{N} \mathcal{F}_n e^{j\,h\,n\,q_z} \tag{4}$$

where where $\mathcal{F}_n$ the Fourier transforms of the n-th trapezoid.

Since, the bottom linewidth of each trapezoid is calculated from the top linewidth of the trapezoid under it, the tessellation of trapezoids can therefore be described with $N + 2$ parameters: the trapezoids' heights, h; a side-wall angle per trapezoid; and the bottom width of the trapezoid underneath.

As illustrated in Figure 4a, the line profile was modeled with $N = 7$, a reasonable compromise between the accuracy of the model and the computational time. The comparison with the cross-section STEM shown in figure 4b reveals our model is realistically reproducing the overall line profile. In order to account for interfacial roughness, a Debye-Waller (DW) factor was also given as initial parameter for the fitting procedure. Which brings the number of initial paramters to 10 (9 for a stack of seven trapezoid and the DW factor).

C. Genetic algorithm

From the previous section, we can simulate the modulations recorded on the Bragg rods in the context of the DWBA. From there, we apply a strategy similar to the one developed by Hannon *et al.* for CD-SAXS [9].

The approach is based on a genetic and evolutionary algorithm, showing a good convergence performance on large parameter spaces. These algorithms mimic biological evolution using the model parameter sets as the encoding genetic information. Genetic algorithms usually start with a population of candidate solutions. This population goes through *mutation* by exchanging the parameters within the population. This is followed by *selection*. Most suitable off-springs, resulting from the mutation are selected for the next generation. The process is repeated until the desired goodness of fit is achieved. Several algorithms

were tested by Hannon *et al.* and the covariance matrix adaptation evolutionary strategy (CMAES) was the best compromise between efficiency and reliability [9]. This approach is intended to reduce the number of generations and therefore the convergence efficiency. In our procedure, the population size is fixed to 100, significantly higher than the lower bound optimal for 10 parameters. Such large population sizes are desired to improve the global search properties and also the implementation of the parallelization of the strategy, which is targeted in the future. A mutational rate of 10, meaning 10 individuals mixed in each generation, is used in the determination of further evolutionary strategy.

With the CMAES approach, fitting 10 variable parameters converges in 120 seconds. The best extracted profile is displayed in Figure 4a. The robustness of convergence was tested by running the CMAES approach with several randomized initial model parameters; all converged to the same profile.

IV. RESULTS AND DISCUSSION

The best line profile extracted by CD-GISAXS is presented in figure 4a, corresponding to the fit presented in figure 2b. Each trapezoid height h is 5.1 nm, leading to an overall line-height of 35.84 nm and the bottom linewidth ω_0 is 49.8 nm. A cross-section TEM measurement was done in order to get a direct image of the line profile and validate the model extracted with CD-GISAXS.

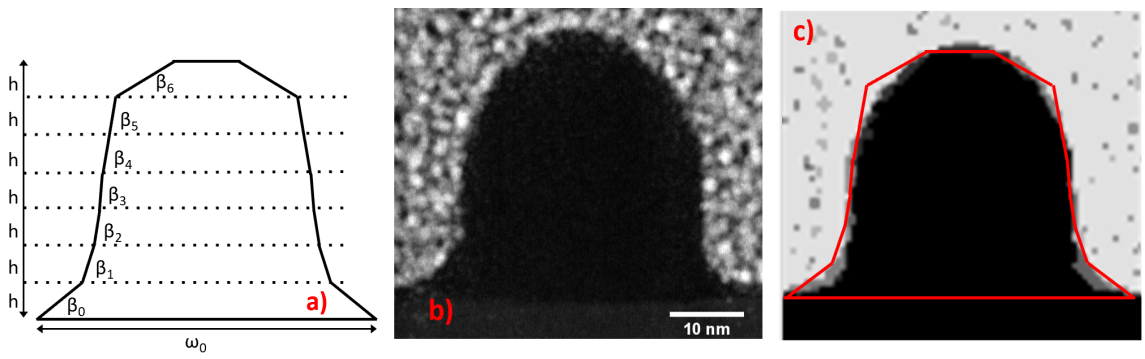

(a) (b) (c)

FIG. 4: a) The line profile determined by CD-GISAXS can be compared with b) the annular dark field image extracted from cross-section STEM and c) a direct comparison between the CD-GISAXS and 3 averaged cross-section STEM profiles.

	ω_0	h	β_0	β_1	β_2	β_3	β_4	β_5	β_6
	nm	*nm*	*deg*	*deg*	*deg*	*deg*	*deg*	*deg*	*deg*
STEM	50.2	5.1	48	74	93	86	82	66	45
CD-GISAXS	49.8	5.1	48	74	84	87	82	81	34

TABLE I: Comparison of the parameters of the line profile determined by CD-GISAXS and cross-section STEM.

The overall profiles extracted form CD-GISAXS and cross-section STEM present similarities such as the presence of a footing (i.e., a wider width at the bottom of the line at the substrate interface) and the presence of a rounding effect at the top of the line. Both of these aspects of the line shape are common for the grating generated by e-beam lithography [7]. However, although the overall profile extracted with CD-GISAXS is quite similar with the STEM image, a closer inspection reveals some mismatches. These mismatches can partly be attributed to our definition of the line profile. One of our first assumptions was the symmetry of the trapezoids which seems to be incorrect w.r.t. STEM image. Moreover, a stack of 7 trapezoids cannot describe such a smooth rounding effect at the top of the line. However 7 trapezoids seems to be the limit at which increasing the number of trapezoids did not improve the fit anymore and only lead to oversampling the line profile 6.

However, even if the cross-section STEM gave us a good estimate of the line profile, a direct comparison between a single line profile and the profile averaged over several square millimeters leads to another source of error. Indeed, the dispersion of the line profile, present in the sample and illustrated on the cross-section SEM image in figure 5, will impact the CD-GISAXS data, specifically the Yoneda area which is sensitive to the in-depth variation of the electronic density gradient. Our current simulation of a mono-disperse line profile led to two intense and sharp Yoneda peaks, characteristic of the electronic density of the silicon substrate and the average density of the line grating. This is not representative of the experimental data, which present a blurring of Yoneda peaks, characteristic of a dispersion of the profile. Also, the two distinct Yoneda peaks in the experimental data are not observed even in the static GISAXS, thus this is not a result of instability in the air bearing.

The counts in the Yoneda region may be under-reported. This can be due to the count rate exceeding the linear counting regime of the Pilatus detector ($< 10^6$ counts/sec). The

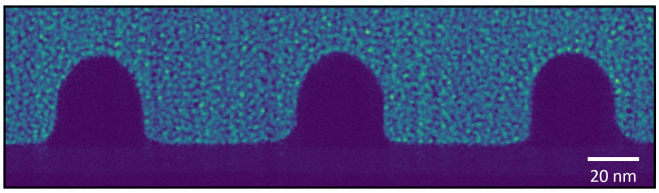

FIG. 5: The cross-section STEM image revealing dispersion on the line profile.

counters are reset after the threshold is reached. Silicon gratings, for all their imperfections, produce very strong Bragg scattering, especially so in the Yoneda region. Such mismatch between our model and the experimental data led us to crop/exclude the Yoneda area form $q_{\|} \in [0, 0.4]$ nm $^{-1}$, in order to allow the convergence of the fit, as illustrated on the figure 2b.

Nevertheless, even though the Yoneda area is not considered for the fit, the region $0.4 \leq q_{\|} \leq 0.5$ nm^{-1} is still not satisfactorily reproduced. This is a residual contribution from the Yoneda area. Therefore, to improve the fit, a dispersion of the line profile needs to be added and is the target of our future work. At the same time, a Monte-Carlo Markov chain algorithm is under development to provide an uncertainty quantification of the extracted profile.

V. CONCLUSION

The reconstruction of the profile of line gratings was performed using small-angle X-ray scattering under a grazing-incidence geometry. The consistency with cross section STEM brings some confidence on the ability of the CD-GISAXS to recreate the line profile. Results such as this open new perspectives to the X-ray scattering techniques to be used as a metrology tool by the semiconductor industry. The main novelty brought by the reflection geometry is the possibility to perform CD-GISAXS with every X-ray energy/wavelength. Therefore, Cu K-α sources and compact X-ray sources operating below 15 keV — otherwise irrelevant for traditional CD-SAXS since the transmission through the wafer is not sufficient — can be used.

The short acquisition time of CD-GISAXS could potentially allow this technique to reach a throughput targeted by the semiconductor industry, even if the beam footprint needs to be reduced to be completely viable for such applications. Additional algorithms for the

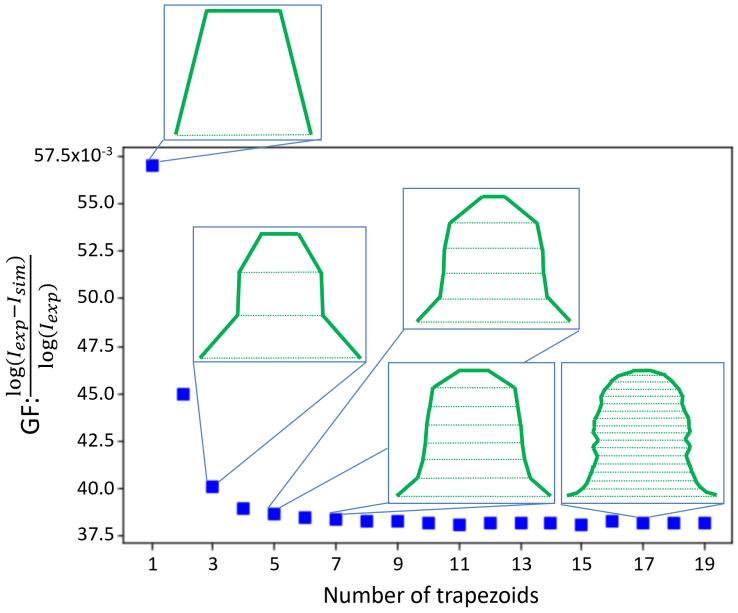

FIG. 6: Evolution of the goodness of fit with model complexity

line profile modeling need to be developed to introduce a dispersion of the line profile and therefore a more realistic description of the sample.

ACKNOWLEDGMENTS

We acknowledge support from the LBNL LDRD program, the DOE Early Career Award program, and the Center for Advanced Mathematics in Energy Research Applications (CAMERA), funded jointly through DOE's ASCR and BES programs. This work used resources of U.S. DOE Office of Science User Facilities, supported under contracts DE-AC02-98CH10886 (National Synchrotron Light Source II, Brookhaven National Lab.), DE-AC02-06CH11357 (Advanced Photon Source, Argonne National Lab.). Experiments performed at the Molecular Foundry, Lawrence Berkeley National Laboratory are supported by the U.S. Department of Energy under contract no. DE-AC02-05CH11231. We thank John Turner of the Molecular Foundry for support of the FIB cross-section sample preparation. We also would like to thank Ruipeng Li for helping tremendously with early

CD-GISAXS measurements at CMS beamline at NSLS-II.

---

[1] R. Silver, T. Germer, R. Attota, M. B. Barnes, B. Bunday, J. Allgair, E. Marx, and J. Jun, Fundamental limits of optical critical dimension metrology: A simulation study, Proc. SPIE **6518**, 65180U (2007).

[2] B. D. Bunday, T. A. Germer, V. Vartanian, A. Cordes, A. Cepler, and C. Settens, Gaps analysis for cd metrology beyond the 22nm node, Proc. SPIE **8681**, 8681 (2013).

[3] B. D. Bunday, D. K. Michelson, J. A. Allgair, A. Tam, D. Chase-Colin, A. Dajczman, O. Adan, and M. Har-Zvi, Cd sem metrology macro cd technology: beyond the average, Proc.SPIE **5752**, 5752 (2005).

[4] K. Ueda, T. Mizuno, and K. Setoguchi, High accuracy cd matching monitor for cd-sem beyond 20nm process, Proc. SPIE **8681**, 8681 (2013).

[5] International technology roadmap for semiconductors, (2013).

[6] R. L. Jones, T. Hu, E. K. Lin, W.-L. Wu, R. Kolb, D. M. Casa, P. J. Bolton, and G. G. Barclay, Small angle x-ray scattering for sub-100 nm pattern characterization, Appl. Phys. Lett. **83**, 4059 (2003).

[7] D. F. Sunday, M. R. Hammond, C. Wang, W.-L. Wu, R. J. Kline, and G. E. Stein, Three-dimensional x-ray metrology for block copolymer lithography line-space patterns, J. Micro. Nanolithogr. MEMS MOEMS **12**, 12 (2013).

[8] D. F. Sunday, E. Ashley, L. Wan, K. C. Patel, R. Ruiz, and R. J. Kline, Templatepolymer commensurability and directed self-assembly block copolymer lithography, J. Polym. Sci. Pol. Phys. **53**, 595 (2015).

[9] A. F. Hannon, D. F. Sunday, D. Windover, and R. J. Kline, Advancing x-ray scattering metrology using inverse genetic algorithms, Journal of Micro/Nanolithography, MEMS, and MOEMS **15**, 15 (2016).

[10] D. F. Sunday, S. List, J. S. Chawla, and R. J. Kline, Determining the shape and periodicity of nanostructures using small-angle x-ray scattering, J. Appl. Crystallogr. **48**, 1355 (2015).

[11] G. Freychet, C. Cadoux, Y. Blancquaert, S. Rey, M. Maret, and P. Gergaud, A study of lateral roughness evaluation through critical-dimension small angle x-ray scattering (cd-saxs), Proc. SPIE **9778**, 9778 (2016).

[12] J. Reche, M. Besacier, P. Gergaud, Y. Blancquaert, G. Freychet, and T. Labbaye, Programmed lwr metrology by multi-techniques approach, Proc. SPIE **10585**, 10585 (2018).

[13] H. S. Suh, X. Chen, P. A. Rincon-Delgadillo, Z. Jiang, J. Strzalka, J. Wang, W. Chen, R. Gronheid, J. J. D. Pablo, N. Ferrier, M. Doxastakis, and P. Nealey, Characterization of the shape and line-edge roughness of polymer gratings with grazing incidence small-angle x-ray scattering and atomic force microscopy, J. Appl. Crystallogr. **49**, 823 (2016).

[14] P. Mikulik, M. Jergel, T. Baumbach, E. Majkova, E. Pincik, S. Luby, L. Ortega, R. Tucoulou, P. Hudek, and I. Kostic, Coplanar and non-coplanar x-ray reflectivity characterization of lateral w/si multilayer gratings, J. of Phys. D: Appl. Phys. **34**, A188 (2001).

[15] M. Yan and A. Gibaud, On the intersection of grating truncation rods with the ewald sphere studied by grazing-incidence small-angle x-ray scattering, J. Appl. Crystallogr. **40**, 1050 (2007).

[16] T. Hofmann, E. Dobisz, and B. M. Ocko, Grazing incident small angle x-ray scattering: A metrology to probe nanopatterned surfaces, J. Vac. Sci. Technol. B Microelectron. Nanometer. Struct. Process. Meas. Phenom. **27**, 3238 (2009).

[17] X. Lu, K. G. Yager, D. Johnston, C. T. Black, and B. M. Ocko, Grazing-incidence transmission x-ray scattering: surface scattering in the born approximation, J. Appl. Crystallogr. **46**, 165 (2013).

[18] V. Soltwisch, J. Wernecke, A. Haase, J. Probstand, M. Schoengen, M. Krumrey, and F. Scholze, Nanometrology on gratings with gisaxs: Fem reconstruction and fourier analysis, Proc. SPIE **9050**, 9050 (2014).

[19] G. Freychet, D. Kumar, R. Pandolfi, D. Staacks, P. Naulleau, R. J. Kline, D. Sunday, M. Fukuto, J. Strzalka, and A. Hexemer, Critical-dimension grazing incidence small angle x-ray scattering, Proc. SPIE **10585**, 10585 (2018).

[20] G. Freychet, I. A. Cordova, T. McAfee, D. Kumar, R. J. Pandolfi, C. Anderson, S. D. Dhuey, P. Naulleau, C. Wang, and A. Hexemer, Reconstructing the three-dimensional latent image of extreme ultraviolet resists with resonant soft x-ray scattering, J. Micro. Nanolithogr. MEMS MOEMS **18**, 1 (2019).

[21] L. A. Giannuzzi and F. A. Stevie, eds., *Introduction to Focused Ion Beams: Instrumentation, Theory, Techniques and Practice* (Springer, 2005).

[22] E. F. Manley, J. Strzalka, T. J. Fauvell, N. E. Jackson, M. J. Leonardi, N. D. Eastham, T. J.

Marks, and L. X. Chen, In situ giwaxs analysis of solvent and additive effects on ptb7 thin film microstructure evolution during spin coating, Adv. Mater. **29**, a129 (2017).

[23] G. Freychet, M. Maret, R. Tiron, X. Chevalier, A. Gharbi, M. FernandezRegulez, and P. Gergaud, Removal of poly(methyl methacrylate) in diblock copolymers films studied by grazing incidence smallangle xray scattering, J. Polym. Sci. Pol. Phys. **54**, 1137 (2016).

[24] S. K. Sinha, E. B. Sirota, S. Garoff, and H. B. Stanley, x-ray and neutron scattering from rough surfaces, Phys. Rev. B **38**, 2297 (1988).

[25] G. Renaud, R. Lazzari, and F. Leroy, Probing surface and interface morphology with grazing incidence small angle x-ray scattering, Sur. Sci. Rep. **64**, 255 (2009).

[26] R. Lazzari, *IsGISAXS*: a program for grazing-incidence small-angle x-ray scattering analysis of supported islands, J. Appl. Crystallogr. **35**, 406 (2002).

[27] S. T. Chourou, A. Sarje, X. S. Li, E. R. Chan, and A. Hexemer, *HipGISAXS*: a high-performance computing code for simulating grazing-incidence x-ray scattering data, J. Appl. Crystallogr. **46**, 1781 (2013).